Articles in PresS. J Neurophysiol (September 27, 2006). doi:10.1152/jn.00589.2006

JN-00589-2006 R2

Excitatory muscarinic modulation strengthens virtual nicotinic synapses on sympathetic neurons and thereby enhances synaptic gain

Paul H.M. Kullmann and John P. Horn

Department of Neurobiology and Center for the Neural Basis of Cognition, University of Pittsburgh School of Medicine, Pittsburgh, Pennsylvania 15261

Running Head: Muscarinic modulation of virtual nicotinic synapses

Contact Information: P.H.M. Kullmann, Department of Neurobiology, University of Pittsburgh School of Medicine, E 1440 Biomedical Science Tower, Pittsburgh, PA, 15261, U.S.A. Email: pkullman@pitt.edu

Copyright © 2006 by the American Physiological Society.

Abstract

Acetylcholine excites many neuronal types by binding to postsynaptic m1-muscarinic receptors that signal to ion channels through the $G_{q/11}$ protein. To investigate the functional significance of this metabotropic pathway in sympathetic ganglia, we studied how muscarinic excitation modulated the integration of virtual nicotinic EPSPs created in dissociated bullfrog B-type sympathetic neurons with the dynamic clamp technique. Muscarine (1 μM) strengthened the impact of virtual synapses by reducing the artificial nicotinic conductance required to reach the postsynaptic firing threshold from 20.9 ± 5.4 nS to 13.1 ± 3.1 nS. Consequently, postganglionic action potential output increased by 4 – 215% when driven by different patterns of virtual presynaptic activity that were chosen to reflect the range of physiological firing rates and convergence levels seen in amphibian and mammalian sympathetic ganglia. In addition to inhibiting the M-type K^+ conductance, muscarine activated a leak conductance in 3 of 37 cells. When this leak conductance was reproduced with the dynamic clamp, it also acted to strengthen virtual nicotinic synapses and enhance postganglionic spike output. Combining pharmacological M-conductance suppression with virtual leak activation, at resting potentials between -50 and -55 mV, produced synergistic strengthening of nicotinic synapses and an increase in the integrated postganglionic spike output. Together, these results reveal how muscarinic activation of a branched metabotropic pathway can enhance integration of fast EPSPs by modulating their effective strength. The results also support the hypothesis that muscarinic synapses permit faster and more accurate feedback control of autonomic behaviors by generating gain through synaptic amplification in sympathetic ganglia.

Key words: dynamic clamp; M-type K^+ conductance; autonomic nervous system

Introduction

The synaptic release of acetylcholine co-activates nicotinic and muscarinic receptors in sympathethic ganglia, initiating a fast nicotinic EPSP and slow muscarinic events that include an EPSP, an IPSP and presynaptic inhibition (Eccles and Libet 1961; Libet and Tosaka 1969; Shen and Horn 1996). Here we examine how postsynaptic muscarinic excitation modulates the integration of nicotinic EPSPs arising from preganglionic synapses that converge on sympathetic neurons. To simplify the experimental analysis, virtual nicotinic EPSPs were created on secretomotor B-type bullfrog sympathetic neurons using the dynamic clamp method (Kullmann et al. 2004). This permitted us to probe the consequences of postsynaptic muscarinic excitation with computer-generated fast synaptic conductance changes whose strength and timing could be precisely controlled and then reproduced in different cells.

Muscarinic excitation of sympathetic B neurons is mediated by suppression of M-type K^+ conductance (gK_M) (Adams and Brown 1982; Brown and Adams 1980) and activation of a cationic leak conductance (g_{leak}) (Kuba and Koketsu 1976; Tsuji and Kuba 1988). In mammals, this pathway includes m1-muscarinic receptors (Marrion et al. 1989) coupled through lipid hydrolysis (Zhang et al. 2003) to M-channels composed of KCNQ2/3 subunits (Selyanko et al. 2002; Shapiro et al. 2000; Wang et al. 1998). Early studies of amphibian B neurons demonstrated that a net decrease in membrane conductance causes muscarinic excitation (Weight and Votava 1970), leading to the proposal that this mechanism could potentiate fast EPSP amplitudes (Schulman and Weight 1976). Subsequent discovery of gK_M and its voltage-dependence revealed that muscarinic excitation increases postsynaptic excitability, as manifest byrepetitive firing

in response to depolarizing stimuli (Brown and Adams 1980). However, the consequences for ganglionic integration of enhanced fast EPSP amplitude and repetitive firing have remained unclear. This problem's significance extends beyond autonomic ganglia.

Muscarinic excitation also occurs in the cerebral cortex (McCormick and Prince 1985), hippocampus (Cole and Nicoll 1984; Dodd et al. 1981) and striatum (Shen et al. 2005). In these circuits, it promotes repetitive firing and oscillatory activity during various physiological and disease states, including memory retrieval (Hasselmo and McGaughy 2004), motor activation (Shen et al. 2005) and epilepsy (Biervert et al. 1998; Cooper et al. 2000; Cooper et al. 2001; Singh et al. 1998). However, the complexity of brain circuits makes it difficult to understand in detail how muscarinic regulation of repetitive firing in single cells shapes circuit dynamics (Cobb and Davies 2005).

Our analysis of muscarinic modulation utilizes a theory of ganglionic integration that reduces circuit behavior to that of a single cell (Karila and Horn 2000) together with dynamic clamp tools capable of testing the theory (Kullmann et al. 2004). Interestingly, previous simulations of a conductance-based model sympathetic neuron predicted that muscarinically enhanced repetitive firing would not influence ganglionic integration (Schobesberger et al. 1999; Schobesberger et al. 2000; Wheeler et al. 2004). Instead, they suggested that muscarine would strengthen subthreshold nicotinic EPSPs and increase synaptic amplification of preganglionic activity (Schobesberger et al. 2000; Wheeler et al. 2004). We now describe new dynamic-clamp experiments to test these ideas using up to ten independent converging nicotinic synapses together with bath-applied muscarine and a virtual cationic leak conductance.

Materials and Methods

All experiments were done on enzymatically dissociated sympathetic B-type neurons from bullfrog (*Rana catesbeiana*) paravertebral ganglia 9 and 10, maintained in culture for up to 2 weeks at room temperature (23^{o}C) on glass coverslips coated with poly-D-lysine (Wheeler et al. 2004). The ganglia were obtained from adult bullfrogs (males and females, 5 – 7 inches) that were killed by rapid brainstem transection and double-pithing in a procedure approved by the Institutional Animal Care and Use Committee at the University of Pittsburgh.

Electrophysiological recordings and dynamic-clamp

Whole-cell perforated-patch recordings were made at room temperature using polished pipettes (1 – 5 MΩ) and amphotericin-B as the ionophore. Details of the dynamic clamp system have been described elsewhere (Kullmann et al. 2004). Briefly, the system included an Axoclamp 2B amplifier (Molecular Devices, Sunnyvale, CA), an embedded Pentium III controller running under a real-time operating system (National Instruments, Austin, TX), a Windows-based host computer and G-clamp version 1.2 software (http://hornlab.neurobio.pitt.edu) written in the LabVIEW-RT 6.1 programming environment (National Instruments). The pipette access resistance (5 – 15 MΩ) was monitored throughout each experiment and compensated using the bridge circuitry of the current-clamp amplifier. Dynamic-clamp measurements were performed at a feedback loop rate of 20 kHz and filtered at 3 kHz. Conventional current-clamp data were sampled at 10 kHz and filtered at 3 kHz, while slow voltage-clamp measurements of steady-state

I-V data were sampled at 5 kHz and filtered at 1 kHz R_{leak} was determined as the slope of the linear part of the IV-relation, typically in the range –65 to –85 mV.

Virtual nicotinic synapses were implemented according to $I_{syn}(t) = k * g_{syn}(t) * (V_M – E_{rev})$. Synaptic conductance as a function of time, $g_{syn}(t)$, was modeled as the sum of two exponentials, used to fit experimentally measured synaptic currents, with time constants of 1 ms for the rising phase and 5 ms for the falling phase (Schobesberger et al. 2000). The synaptic reversal potential, E_{rev}, was set to 0 mV (Shen and Horn 1995) and synaptic strength was controlled by adjusting the dimensionless scaling factor k. Threshold-g_{syn}, defined as the synaptic conductance required to trigger an action potential, was determined with an automated binary search routine that delivered virtual nicotinic EPSPs at a rate of 0.5 Hz (Kullmann et al. 2004). By systematically varying the peak amplitude of the synaptic conductance based on its ability to trigger an action potential, the search routine generally found threshold-g_{syn} within 10 trials. During this process, the dynamic clamp continually measured membrane potential, $V_{M,}$ calculated the appropriate synaptic current, I_{syn}, and injected it into the cell (Kullmann et al. 2004).

The virtual leak conductance, g_{leak}, used to mimic the leak component of muscarinic excitation was implemented as time and voltage invariant with a reversal potential of 0 mV (Schobesberger et al. 2000; Tsuji and Kuba 1988).

To create patterns of virtual nicotinic EPSPs that mimic activity *in vivo*, the timing of synaptic events was modeled as Poisson process (Karila and Horn 2000; Wheeler et al. 2004) with Neurosim 2.1 (http://hornlab.neurobio.pitt.edu), a MATLAB program written by Dr. D.W. Wheeler. The program generated the required random numbers and constructed conductance waveforms describing activity of one strong

primary synapse and a specified number of weak secondary synapses. During each experiment, G-clamp then scaled the primary and secondary conductance template files relative to threshold-g_{syn}, as measured for each cell, before combining them into one final template that commanded the dynamic-clamp and measured synaptic gain (Wheeler et al. 2004). Scaling of conductance templates was based on the mean value of at least 3 consecutive measurements of threshold-g_{syn}. Conductance templates with a mean rate of synaptic activity of 5 Hz were 40 s long (~200 events per synapse), while templates with a mean rate of 0.5 Hz were 60 – 200 s long (~30 – 100 events per synapse).

Solutions and chemicals

The Ringer solution contained (in mM): 115 NaCl, 2 KCl, 1.8 $CaCl_2$, and 4 NaHEPES, adjusted to pH 7.3. The pipette solution contained (in mM): 110 potassium gluconate, 10 NaCl, and 5 NaHEPES, adjusted to pH 7.2. Patch pipettes were backfilled with this solution plus 250 µg/ml amphotericin-B (Sigma-Aldrich, St. Louis, MO). (-)-Muscarine chloride was also obtained from Sigma-Aldrich.

Data analysis

In vivo synaptic input to sympathetic neurons generally consists of one strong synapse, known as the primary, which invariably elicits an action potential, and a variable number of weak, sub-threshold synapses, known as secondaries (Karila and Horn 2000). For simplicity, it was assumed that primary and secondary synapses originate from a common population of preganglionic neurons and therefore that all synapses are active at the same mean rate. As in previous work, synaptic gain was defined as the mean postsynaptic

firing rate divided by the mean firing rate of virtual presynaptic neurons (Karila and Horn 2000; Wheeler et al. 2004). In this scheme, when action potentials are generated solely by the strong primary synapse, the synaptic gain is 1 and when additional action potentials are generated by summation of secondary EPSPs the gain rises above 1. Synergy between gK_M and g_{leak} was calculated as the difference between the reduction in threshold-g_{syn} for the combined conductance changes and that for the sum of their individual effects, divided by the latter and multiplied by 100 (Schobesberger et al. 2000). If, for example, the combined conductances reduced threshold-g_{syn} by 3 nS and the individual effects were 1nS each, then this would correspond to a synergy of 50% (100*(3 nS -2 nS)/2 nS)).

Action potential threshold was measured as the maximum second derivative of membrane potential with respect to voltage in phase space (method II in (Sekerli et al. 2004)).

Grouped data and error bars in figures reflect the mean ± SEM, except in Fig. 4C where the error bars indicate standard deviations. Single statistical comparisons between grouped data were made using two-sided t-tests, while multiple comparisons were conducted with a repeated measurements ANOVA and Tukey's test. $P<0.05$ was the criterion for significance.

Results

Muscarine strengthens nicotinic synapses by enhancing excitability

In principle, muscarinic EPSPs could serve to modulate ganglionic integration by enhancing the efficacy of nicotinic synapses or by allowing nicotinic EPSPs to drive repetitive postsynaptic firing (Brown and Adams 1980; Schulman and Weight 1976). To distinguish between these possibilities we examined how muscarine modulated the postsynaptic response to virtual nicotinic EPSPs of defined strength.

Bath-applied muscarine increased the efficacy of virtual nicotinic synapses by lowering threshold-g_{syn} in a manner that was reversible (Fig. 1A-C)and dose-dependent. Fifty nM muscarine reduced threshold-g_{syn} to 87.9 ± 4.0 % of control (3 cells), 1 μM muscarine reduced threshold-g_{syn} to 63.7 ± 2.6 % of control (26 cells, $P<0.002$, paired t-test)), and 30 μM muscarine reduced threshold-g_{syn} to 37.2 ± 2.3 % (4 cells). For 1 μM muscarine, where most data were obtained, the reduction in threshold-g_{syn} ranged between 31.3 and 86.0% from a mean of 20.9 ± 5.4 nS in control Ringer to 13.1 ± 3.1 nS in muscarine. These effects could not be explained by a hyperpolarizing shift in the threshold membrane potential for spike initiation (Fig. 1A), an action thatone might expect to enhance excitation by fast EPSPs. To the contrary, 1 μM muscarine caused a slight depolarization of action potential threshold from -22.4 ± 1.3 mV to -21.4 ± 1.4 mV (24 cells, $P<0.01$, paired t-test). Washout of theagonist often resulted in a transient over-recovery of threshold-g_{syn} (Fig. 1B), whose time course resembled the well known over-recovery of gK_M seen after its metabotropic suppression (Pfaffinger 1988; Tokimasa et al. 1996).

In addition to reducing threshold-g_{syn}, 1 μM muscarine depolarized V_{rest} (Fig. 1D) by 6.5 ± 0.7 mV (26 cells), thereby mimicking the slow EPSP recorded from intact ganglia. Although it could be argued that the muscarinic reduction in threshold-g_{syn} arises simply from membrane depolarization, the correlation between these two effects (Fig. 1E) was weak ($r^2 = 0.253$, $P < 0.01$, Pearson correlation test). Previous computational simulations indicate that this behavior originates from the non-linear voltage- and time-dependent gating of gK_M interacting with the resting leak conductance (Schobesberger et al. 2000). In order to test the idea that membrane depolarization could not fully account for the muscarinic effect upon threshold-$g_{syn,}$ an additional set of experiments was run in which steady current injection was used first to null out the depolarization caused by muscarine and then after washout to mimic the depolarization (Fig. 2A,B). In 7 of 7 cells, injection of hyperpolarizing current reduced but did not eliminate the reduction of threshold-g_{syn} by muscarine. In these same cells, simple injection of depolarizing current also reduced threshold-g_{syn}, but not to the same extent as muscarine. In addition to these tests, we examined in three of these cells how muscarine and current injection influenced the shape of subthreshold virtual nicotinic EPSPs (Fig. 2C, D). In every cell, muscarine had very little effect upon fast EPSP amplitude while causing a lengthening of EPSP duration. These results confirm the prediction from previous numerical simulations of the same experiment (see Fig. 2 in Schobesberger et al., 1999).

Unlike the robust effect of muscarinic excitation upon the efficacy of nicotinic stimulation, virtual fast EPSPs never initiated repetitive firing of action potentials either in control Ringer or after exposure to muscarine (Figs. 1A, 5B, 7A). Nonetheless, B

neurons were capable of repetitive firing. Their normal propensity to fire a single action potential in response to a rectangular pulse of depolarizing constant-current was readily converted to repetitive firing by addition of muscarine (Fig. 3A). Indeed the conversion from phasic to tonic firing constitutes the classic signature of muscarinic excitation (Adams et al. 1982). In a few cells, the depolarization produced by high muscarine concentrations $\geq$ 10 μM led to spontaneous firing, but this behavior did not require nicotinic or any other form of stimulation.

Previous studies indicate that muscarine activates a branched signaling pathway in bullfrog B neurons to suppress gK_M and activate g_{leak} (Tsuji and Kuba 1988). To assess whether both conductance changes occurred under our experimental conditions, steady-state I-V relations were constructed with either voltage-clamp or current-clamp measurements, which yielded similar data. In 34 of 37 cells, muscarine only inhibited gK_M, which was evident in the I-V relation as a voltage-dependent inward current activated positive to -70 mV (Fig. 3B). In the 3 other neurons, the muscarinic current had two components corresponding to suppression of I_M and activation of an inward leak conductance (0.98 ± 0.56 nS) with an extrapolated reversal potential of -20 ± 9.3 mV (Fig. 3C). In all 3 cells, the leak component of the muscarininc response recovered upon washout, thereby indicating it was not an artifact of cell damage or deterioration. Both the increase in leak conductance and the decrease in M-conductance had the effect of linearizing the I-V relation in the region between the resting potential (-55 to -70 mV) and the spike threshold (-20 to -30 mV). This resulted in depolarization and a reduction of the inward synaptic current required to reach threshold for generating an action potential.

The next set of experiments examined how gK_M and g_{leak} interact to control the efficacy of virtual nicotinic EPSPs. To assess the impact of each conductance type, we exploited the fact that most neurons in our preparations did not exhibit the muscarinically controlled g_{leak}. Instead we used the dynamic clamp to implement a virtual leak response in neurons that responded to bath-applied muscarine with a pure gK_M response. This approach permitted independent manipulation of the two conductances. In the experiment illustrated in Fig. 4A, threshold-g_{syn} was measured repeatedly in the presence and absence of a small virtual g_{leak} (0.25 nS). Plotting these data against time yielded one baseline describing threshold-g_{syn} without the leak and a second lower baseline, which reflected the ability of the leak to reduce threshold-g_{syn}. Upon application of muscarine both baselines shifted to lower values, but the difference between them increased. This was because muscarine had a greater effect in the presence of the leak conductance. In other words, the increase in g_{leak} and reduction in gK_M interacted synergistically to reduce threshold-g_{syn}. This experimental protocol was repeated 25 times in 15 neurons using different levels of virtual g_{leak} (0.1 – 1 nS) comparable to those activated by a muscarinic agonist (Tsuji and Kuba 1988). Figure 4B illustrates grouped data from 11 of these trials, collected from 7 neurons where the interaction between g_{leak} and gK_M was synergistic. In these cases, adding g_{leak} alone reduced threshold-g_{syn} to 90.1 ± 2.1 % of control and suppressing gK_M alone reduced threshold-g_{syn} to 81.4 ± 3.7 % of control, while combining the two changes reduced threshold-g_{syn} to 63.9 ± 4.3 % of control, which was a greater change than the arithmetic sum of the two individual effects (71.5 ± 3.9 % of control). This behavior contrasted to the other 14 trials where no synergy or slight negative synergy was seen. Comparing the positive and negative synergy data (Fig. 4C)

revealed a significant difference in resting membrane potentials under control conditions prior to manipulation of g_{leak} and gK_M (positive synergy: -54.4 ± 1.8 mV; negative synergy: –63.4 ± 1.4 mV; $P < 0.001$; two-tailed unpaired t-test). The likely explanation again derives from the voltage-dependence of gK_M (Schobesberger et al. 2000). Hyperpolarized resting potentials are associated with low activation of gK_M, while more depolarized resting potentials can fall into a region where small depolarizations cause large activation of gK_M (Fig. 3B). Accordingly, the effects of g_{leak} and gK_M should add supralinearly when the depolarization produced by the leak causes a large increase in the resting M-current. To test this idea, synergy was measured in 4 cells with low resting potentials and then a second time after steady currents were injected to produce small depolarizations (Fig. 4D). In all four cases, depolarization led to an increase in synergy between g_{leak} and gK_M as assayed by the reduction in threshold-g_{syn}.

Muscarinic modulation of synaptic gain

Synaptic amplification of activity can arise in sympathetic ganglia from the summation of fast nicotinic EPSPs that are subthreshold in strength (Karila and Horn 2000; Wheeler et al. 2004). Finding that muscarinic excitation enhanced the effective strength of nicotinic synapses therefore implies a concomitant increase in synaptic gain. To test this prediction, B neurons were stimulated with defined patterns of noisy virtual nicotinic synaptic input in the presence and absence of muscarine (Fig. 5). The templates of virtual synaptic conductance used to drive the dynamic clamp and measure synaptic gain were defined by parameters describing nicotinic convergence, the strength of nicotinic synapses, and the mean firing rate of preganglionic neurons. Specific values for

these parameters were chosen to be physiologically realistic and to span a range of conditions that elicit different baseline levels of synaptic gain in simulations and dynamic-clamp recordings (Karila and Horn 2000; Wheeler et al. 2004). All synaptic templates incorporated the *n+1* pattern of nicotinic convergence seen in paravertebral sympathetic ganglia (Karila and Horn 2000). To reproduce this pattern, each template contained 3 or 9 secondary synapses whose resting strength was set to either 50% or 90% of threshold-g_{syn} and 1 primary synapse whose strength was always set to 10 times threshold-g_{syn}. Similarly, the average presynaptic firing rate was studied at 0.5 Hz and 5 Hz to reflect a physiologically relevant range.

By testing individual cells with different patterns of virtual synaptic stimulation, we found that muscarine elevated synaptic gain over the entire parameter space for preganglionic activity (Figs. 5, 6). In order to obtain reliable estimates of synaptic gain, it was essential to maintain stable recordings for periods long enough to permit repeated trials, interleaving of different stimulus templates, applications of muscarine, and recovery between trials. The cell illustrated in Fig. 5 was tested 9 times in this way over a period of 80 minutes. In this particular experiment, all synaptic templates contained 9 secondary nicotinic synapses firing at 5 Hz, but their strength was varied during repeated trials. The results from this cell showed that muscarine reproducibly elevated synaptic gain. In replicate trials with secondary synaptic strength set at 50% threshold-g_{syn}, 1 μM muscarine increased gain in this cell from 0.97 and 0.99 to 1.33 and 1.35. When secondary synaptic strength was raised to 90% threshold-$g_{syn,}$ muscarine increased gain from 1.31 and 1.33 to 1.77 and 1.88. Synaptic gain dropped to slightly less than 1 when secondary synapses were turned off by setting their strength to 0. The drop in gain below

1 has been found in other recent experiments to arise from the failure of large EPSPs to trigger firing during the refractory period after each spike (Wheeler et al. 2004). After each stimulus trial we also observed transient changes in threshold-g_{syn}, but rest periods successfully allowed for recovery back to baseline before the next trial (Fig. 5A). In grouped data (Fig. 6B) using the same stimulus parameters (f_{pre} = 5 Hz, 9 secondary synapses), the increase in synaptic gain produced by 1-5 μM muscarine was significant when secondary synaptic strength was set to 50% threshold-g_{syn} (control 1.054 ± 0.028, muscarine 1.227 ± 0.028, 9 cells, $P<0.05$, paired t-test) and to 90% threshold-g_{syn} (control 1.467 ± 0.051, muscarine 1.759 ± 0.064, 10 cells, $P<0.05$, paired t-test).

Using the same approach, we systematically tested the effect of muscarine upon synaptic gain elicited by other preganglionic stimuli. With only 3 secondary synapses and f_{pre} maintained at 5 Hz, muscarine elevated gain (Fig. 6A) from 0.926 ± 0.005 to 0.960 ± 0.018 (50% threshold-g_{syn}, 6 cells; $P<0.05$, paired t-test) and from 1.003 ± 0.026 to 1.164 ± 0.056 (90% threshold-g_{syn} 11 cells; $P<0.05$, paired t-test). The largest muscarinic effects, which doubled synaptic gain, were recorded when f_{pre} was lowered to 0.5 Hz and secondary synapses were scaled to 90% threshold-g_{syn} (Fig. 6C, D). With 3 secondary synapses, muscarine increased the gain under these conditions from 1.268 ± 0.100 to 2.556 ± 0.130 (6 cells; $P<0.05$, paired t-test) and with 9 secondary synapses, muscarine increased the gain from 2.609 ± 0.340, to 5.615 ± 0.842 (5 cells; $P<0.05$, paired t-test). Smaller effects were recorded with 0.5 Hz stimulation and secondary synapses scaled to 50% threshold-g_{syn} (Fig. 6C, D). With 3 secondary synapses, muscarine increased synaptic gain from 1.037 ± 0.001 to 1.300 ± 0.144 (3 cells) and with

9 secondary synapses, muscarine increased synaptic gain from 1.432 ± 0.070 to 1.784 ± 0.157 (3 cells).

Synergistic regulation of synaptic gain by gK_M and g_{leak}

In the preceding experiments (Figs. 5, 6), metabotropic suppression of gK_M was the most likely mechanism for enhancement of synaptic gain because 92% of the neurons in our cultures did not show the muscarinically activated leak conductance. Nonetheless, the analysis of excitability showed clearly that introduction of a virtual leak conductance could lower threshold-g_{syn} and interact synergistically with suppression of gK_M in regulating the response to nicotinic excitation (Fig. 4). A final series of experiments examined whether these effects could also produce significant increases in synaptic gain. B neurons were stimulated with a synaptic template that included 3 secondary synapses set to 50% threshold-g_{syn}, 1 primary synapse and an average presynaptic firing rate of 0.5 Hz. With this template, separate introduction of either the virtual g_{leak} or muscarine each produced small increases in synaptic gain, and adding both together produced a significant increase in gain, greater than the sum of the individual effects (Fig. 7). In grouped data from 5 neurons, synaptic gain was 1.069 ± 0.008 under control conditions. Adding 0.25 to 0.5 nS of virtual g_{leak} increased the gain to 1.169 ± 0.020, while reducing R_{leak} in the steady-state I-V relation from 1108 ± 92 MΩ to 834 ± 67 MΩ and depolarizing the resting potential from –68.6 ± 1.4 mV to –54.1 ± 2.2 mV. Adding 1 μM muscarine increased synaptic gain to 1.214 ± 0.055 and depolarized the cells from –67.1 ± 0.9 mV to –60.6 ± 1.7 mV. Adding the virtual leak and muscarine together increased

synaptic gain to 1.794 ± 0.276 ($P<0.05$, repeated measurement ANOVA, Tukey's post-hoc test) and depolarized the cells from –66.1 ± 1.2 mV to –46.8 ± 3.1 mV.

Discussion

In this study, we analyzed the integrative role of muscarinic excitation in sympathetic ganglia by testing the predictions of a computational model (Schobesberger et al. 2000; Wheeler et al. 2004). To simplify the experimental problem, the dynamic clamp method was used to create virtual nicotinic synapses whose strength, number and activity could be precisely controlled. The results show that muscarinic suppression of gK_M and activation of a virtual g_{leak} are each sufficient to strengthen the excitatory impact of nicotinic synapses by lowering threshold-g_{syn} (Figs. 1, 4). Importantly, the excitatory action of muscarine cannot be explained simply by its depolarizing effect on resting potential (Fig. 2). A direct consequence of excitatory muscarinic modulation in this system is to increase the synaptic gain (Figs. 5 - 7) that arises through convergence of nicotinic synapses on sympathetic neurons. Both effects were very robust. Although variable in magnitude, the excitatory consequences of muscarinic modulation were consistently evoked over an entire parameter space whose boundaries were chosen to reflect physiological estimates of naturally occurring synaptic strength, nicotinic convergence and preganglionic activity. Our data also show that combining the changes in gK_M and g_{leak} can result in a synergy to produce even larger increases in synaptic strength (Fig. 4) and gain (Fig. 7). These non-linear interactions between gK_M and g_{leak} arise from the voltage and time-dependence of gK_M. Finally, the results indicate that nicotinic excitation does not act as a physiological trigger of repetitive firing, even though sympathetic neurons are capable of such firing during metabotropic excitation (Fig. 3, also see Adams et al. 1982; Dodd and Horn 1983)

The bridge from metabotropic signaling to synaptic integration

The problem of muscarinic modulation in autonomic ganglia is long-standing and multifaceted. Slow muscarinic EPSPs were first recorded in the 1960's from isolated preparations of the rabbit superior cervical ganglion (Eccles and Libet 1961; Libet and Tosaka 1969) and amphibian lumbar chain ganglia (Koketsu 1969; Nishi and Koketsu 1968; Tosaka et al. 1968). It took ten years to implicate a decrease in K^+ conductance (Weight and Votava 1970) and another ten to elucidate the voltage-dependent nature of the M-conductance (Brown and Adams 1980). Most subsequent work focused on the signal transduction pathway, which is now best understood in mammalian sympathetic neurons. Muscarinic suppression of gK_M arises through the m1 subclass of receptors (Marrion et al. 1989), which are coupled to the $G_{q/11}$ protein, activation of phospholipase C (Delmas et al. 2004), hydrolysis of PIP_2 (Suh and Hille 2002; Suh et al. 2004; Zhang et al. 2003) and reduced opening of channels composed of KCNQ2 and KCNQ3 subunits (Delmas et al. 2004; Selyanko et al. 2002; Selyanko et al. 2000; Shapiro et al. 2000; Wang et al. 1998). By comparison, muscarinic activation of g_{leak} in paravertebral sympathetic neurons has been documented repeatedly (Kuba and Koketsu 1976; Mochida and Kobayashi 1986; Tsuji and Kuba 1988), but further details have remained elusive. Possible candidates for this conductance include cyclic nucleotide-gated ion channels (Thompson 1997) and transient receptor potential (trp) channels (Delmas et al. 2004). However, it remains unclear why muscarinic activation of the leak was only seen in 8% of the B neurons that we studied. The rarity of these cells could reflect either a functionally specialized subset of sympathetic B neurons or a technical limitation of our tissue culture and recording methods. In any event, it is important to note that various

forms of branched metabotropic signaling pathways are widespread. The observations reported here may therefore prove significant in a number of different cellular contexts.

Previous efforts to understand the role of slow muscarinic excitation in ganglionic integration have focused largely on the afterdischarge of action potentials that is sometimes associated with the slow EPSP (Horn 1992; Nishi and Koketsu 1968). *In vivo* recordings from lumbar chain ganglia in the cat (Janig 1995) and frog(Ivanoff and Smith 1997) have demonstrated afterdischarges and slow potentials, but this approach has not elucidated a physiological role for such events, due in part to problems that arise from the difficulty of working *in vivo* and the need to introduce exogenous drugs and nerve stimulation to evoke afterdischarges. Another approach was to isolate preparations of amphibian ganglia together with end-organs (Jobling and Horn 1996; Thorne and Horn 1997). This demonstrated that metabotropic excitation of postganglionic neurons could elicit detectable consequences in arteries and cutaneous glands, but again the effects were critically dependent on exogenous drugs such as nicotine and d-tubocurarine. All of these results from earlier work are born out by the present finding that virtual nicotinic EPSPs were incapable of evoking repetitive firing of any kind, let alone the type that has been associated with classical recordings of ganglionic afterdischarges. Nonetheless, our conclusion that metabotropically regulated repetitive firing does not contribute to normal ganglionic integration should not be construed as an argument against the practical utility of classifying cell firing properties as phasic or tonic. Indeed the firing patterns induced by current injection have proven useful as signatures to functionally identify different classes of central and peripheral neurons (Boyd et al. 1996; Cassell et al. 1986; Connors and Gutnick 1990). Our results indicate simply that one must be cautious in

extrapolating from such signatures to synaptic integration. In central neurons where convergence is high and individual synapses produce relatively small EPSPs, varying the background level of synaptic activity may function in a manner analogous to steady current injection and lead to different consequences than observed in sympathetic neurons.

The view of muscarinic excitation developed in this paper has its earliest precedent in the observation that slow EPSPs potentiate the amplitudes of fast EPSPs by reducing total membrane conductance and thereby lowering the shunting of synaptic currents (Schulman and Weight 1976). Although very attractive, the data supporting this idea are in retrospect very minimal and recent simulations indicate that effects on EPSP amplitude would be very small and difficult to detect (Schobesberger et al. 1999). These predictions were indeed confirmed by our observations of fast virtual EPSP shape (Fig. 2C,D). When viewed in the context of synaptic strength, our computational and dynamic clamp approach has now shown clearly for the first time that by altering postsynaptic excitability, muscarinic excitation can strengthen the impact of nicotinic synapses.

By answering some of the original questions about muscarinic modulation it becomes possible to focus on other unresolved issues, both postsynaptic and presynaptic. First there is the limitation of the dynamic clamp method, which implements conductances at the site of recording without mimicking the spatial distribution of synapses over the surface of a neuron. In the case of bullfrog neurons, this problem is insignificant because the cells are monopolar with nicotinic synapses on the soma and axon hillock. In the case of mammalian sympathetic neurons, one must eventually account for the influence of dendrites. Nonetheless, our results demonstrate how

muscarinic excitation can modulate integration of fast EPSPs within an isopotential cellular compartment. A second postsynaptic issue is the possible role of calcium activated K^+ conductances (gK_{Ca}). Although changes in gK_{Ca} do not contribute to the slow muscarinic EPSP, in mammalian sympathetic neurons muscarinic inhibition of N-type calcium currents can reduce their activation by action potentials and may thereby influence synaptic integration (Bernheim et al. 1992; Haley et al. 2000). However, this mechanism is not expressed in bullfrog sympathetic neurons (Bley and Tsien 1990; Jones and Marks 1989) and therefore cannot account for the present results. Finally, it is important to note that our analysis of postsynaptic integration deliberately simplified presynaptic mechanisms by omitting the dynamics of release. It would be interesting to extend the analysis of ganglionic integration to include presynaptic facilitation and depression together with muscarinic receptors that inhibit Ach release (Karila and Horn 2000; Shen and Horn 1996). In the meantime, the present experiments provide evidence that postsynaptic muscarinic excitation can regulate the synaptic gain generated in sympathetic ganglia. The resulting notion that ganglia function as use-dependent amplifiers is likely to be important because the ganglia are embedded in negative feedback loops that control blood pressure, body temperature and other physiological state variables.

Grants: This work was supported by NIH grant RO1 NS21065.

References

Adams PR and Brown DA. Synaptic inhibition of the M-current: slow excitatory post-synaptic potential mechanism in bullfrog sympathetic neurones. *J Physiol* 332: 263-272, 1982.

Adams PR, Brown DA, and Constanti A. Pharmacological inhibition of the M-current. *J Physiol* 332: 223-262, 1982.

Bernheim L, Mathie A, and Hille B. Characterization of muscarinic receptor subtypes inhibiting Ca2+ current and M current in rat sympathetic neurons. *Proc Natl Acad Sci U S A* 89: 9544-9548, 1992.

Biervert C, Schroeder BC, Kubisch C, Berkovic SF, Propping P, Jentsch TJ, and Steinlein OK. A potassium channel mutation in neonatal human epilepsy. *Science* 279: 403-406, 1998.

Bley KR and Tsien RW. Inhibition of Ca2+ and K+ channels in sympathetic neurons by neuropeptides and other ganglionic transmitters. *Neuron* 4: 379-391, 1990.

Boyd HD, McLachlan EM, Keast JR, and Inokuchi H. Three electrophysiological classes of guinea pig sympathetic postganglionic neurone have distinct morphologies. *J Comp Neurol* 369: 372-387, 1996.

Brown DA and Adams PR. Muscarinic suppression of a novel voltage-sensitive K+ current in a vertebrate neurone. *Nature* 283: 673-676, 1980.

Cassell JF, Clark AL, and McLachlan EM. Characteristics of phasic and tonic sympathetic ganglion cells of the guinea-pig. *J Physiol* 372: 457-483, 1986.

Cobb SR and Davies CH. Cholinergic modulation of hippocampal cells and circuits. *J Physiol* 562: 81-88, 2005.

Cole AE and Nicoll RA. Characterization of a slow cholinergic post-synaptic potential recorded in vitro from rat hippocampal pyramidal cells. *J Physiol* 352: 173-188, 1984.

Connors BW and Gutnick MJ. Intrinsic firing patterns of diverse neocortical neurons. *Trends Neurosci* 13: 99-104, 1990.

Cooper EC, Aldape KD, Abosch A, Barbaro NM, Berger MS, Peacock WS, Jan YN, and Jan LY. Colocalization and coassembly of two human brain M-type potassium channel subunits that are mutated in epilepsy. *Proc Natl Acad Sci U S A* 97: 4914-4919, 2000.

Cooper EC, Harrington E, Jan YN, and Jan LY. M channel KCNQ2 subunits are localized to key sites for control of neuronal network oscillations and synchronization in mouse brain. *J Neurosci* 21: 9529-9540, 2001.

Delmas P, Crest M, and Brown DA. Functional organization of PLC signaling microdomains in neurons. *Trends Neurosci* 27: 41-47, 2004.

Dodd J, Dingledine R, and Kelly JS. The excitatory action of acetylcholine on hippocampal neurones of the guinea pig and rat maintained in vitro. *Brain Res* 207: 109-127, 1981.

Dodd J and Horn JP. Muscarinic inhibition of sympathetic C neurones in the bullfrog. *J Physiol* 334: 271-291, 1983.

Eccles RM and Libet B. Origin and blockade of the synaptic responses of curarized sympathetic ganglia. *J Physiol* 157: 484-503, 1961.

Haley JE, Delmas P, Offermanns S, Abogadie FC, Simon MI, Buckley NJ, and Brown DA. Muscarinic inhibition of calcium current and M current in Galpha q-deficient mice. *J Neurosci* 20: 3973-3979, 2000.

Hasselmo ME and McGaughy J. High acetylcholine levels set circuit dynamics for attention and encoding and low acetylcholine levels set dynamics for consolidation. *Prog Brain Res* 145: 207-231, 2004.

Horn JP. The integrative role of synaptic cotransmission in the bullfrog vasomotor C system: evidence for a synaptic gain hypothesis. *Can J Physiol Pharmacol* 70 Suppl: S19-26, 1992.

Ivanoff AY and Smith PA. On the role of muscarinic and peptidergic receptors in ganglionic transmission in bullfrogs in vivo. *Am J Physiol* 272: R1501-1514, 1997.

Janig WM. Ganglionic Transmission *in vivo*. In: *Autonomic Ganglia*, edited by McLachlan EM. Australia: Harwood Academic Publishers, 1995, p. 349-395.

Jobling P and Horn JP. In vitro relation between preganglionic sympathetic stimulation and activity of cutaneous glands in the bullfrog. *J Physiol* 494: 287-296, 1996.

Jones SW and Marks TN. Calcium currents in bullfrog sympathetic neurons. I. Activation kinetics and pharmacology. *J Gen Physiol* 94: 151-167, 1989.

Karila P and Horn JP. Secondary nicotinic synapses on sympathetic B neurons and their putative role in ganglionic amplification of activity. *J Neurosci* 20: 908-918, 2000.

Koketsu K. Cholinergic synaptic potentials and the underlying ionic mechasims. *Fed Proc* 28: 101-112, 1969.

Kuba K and Koketsu K. Analysis of the slow excitatory postsynaptic potential in bullfrog sympathetic ganglion cells. *Jpn J Physiol* 26: 651-669, 1976.

Kullmann PH, Wheeler DW, Beacom J, and Horn JP. Implementation of a fast 16-Bit dynamic clamp using LabVIEW-RT. *J Neurophysiol* 91: 542-554, 2004.

Libet B and Tosaka T. Slow inhibitory and excitatory postsynaptic responses in single cells of mammalian sympathetic ganglia. *J Neurophysiol* 32: 43-50, 1969.

Marrion NV, Smart TG, Marsh SJ, and Brown DA. Muscarinic suppression of the M-current in the rat sympathetic ganglion is mediated by receptors of the M1-subtype. *Br J Pharmacol* 98: 557-573, 1989.

McCormick DA and Prince DA. Two types of muscarinic response to acetylcholine in mammalian cortical neurons. *Proc Natl Acad Sci U S A* 82: 6344-6348, 1985.

Mochida S and Kobayashi H. Three types of muscarinic conductance changes in sympathetic neurons discriminately evoked by the different concentrations of acetylcholine. *Brain Res* 383: 299-304, 1986.

Nishi S and Koketsu K. Early and late after discharges of amphibian sympathetic ganglion cells. *J Neurophysiol* 31: 109-121, 1968.

Pfaffinger P. Muscarine and t-LHRH suppress M-current by activating an IAP-insensitive G-protein. *J Neurosci* 8: 3343-3353, 1988.

Schobesberger H, Gutkin BS, and Horn JP. A minimal model for metabotropic modulation of fast synaptic transmission and firing properties in bullfrog sympathetic B neurons. *Neurocomputing* 26-27: 255-262, 1999.

Schobesberger H, Wheeler DW, and Horn JP. A model for pleiotropic muscarinic potentiation of fast synaptic transmission. *J Neurophysiol* 83: 1912-1923, 2000.

Schulman JA and Weight FF. Synaptic transmission: long-lasting potentiation by a postsynaptic mechanism. *Science* 194: 1437-1439, 1976.

Sekerli M, Del Negro CA, Lee RH, and Butera RJ. Estimating action potential thresholds from neuronal time-series: new metrics and evaluation of methodologies. *IEEE Trans Biomed Eng* 51: 1665-1672, 2004.

Selyanko AA, Delmas P, Hadley JK, Tatulian L, Wood IC, Mistry M, London B, and Brown DA. Dominant-negative subunits reveal potassium channel families that contribute to M-like potassium currents. *J Neurosci* 22: RC212, 2002.

Selyanko AA, Hadley JK, Wood IC, Abogadie FC, Jentsch TJ, and Brown DA. Inhibition of KCNQ1-4 potassium channels expressed in mammalian cells via M1 muscarinic acetylcholine receptors. *J Physiol* 522 Pt 3: 349-355, 2000.

Shapiro MS, Roche JP, Kaftan EJ, Cruzblanca H, Mackie K, and Hille B. Reconstitution of muscarinic modulation of the KCNQ2/KCNQ3 K(+) channels that underlie the neuronal M current. *J Neurosci* 20: 1710-1721, 2000.

Shen W, Hamilton SE, Nathanson NM, and Surmeier DJ. Cholinergic suppression of KCNQ channel currents enhances excitability of striatal medium spiny neurons. *J Neurosci* 25: 7449-7458, 2005.

Shen WX and Horn JP. A presynaptic mechanism accounts for the differential block of nicotinic synapses on sympathetic B and C neurons by d-tubocurarine. *J Neurosci* 15: 5025-5035, 1995.

Shen WX and Horn JP. Presynaptic muscarinic inhibition in bullfrog sympathetic ganglia. *J Physiol* 491: 413-421, 1996.

Singh NA, Charlier C, Stauffer D, DuPont BR, Leach RJ, Melis R, Ronen GM, Bjerre I, Quattlebaum T, Murphy JV, McHarg ML, Gagnon D, Rosales TO, Peiffer A,

Anderson VE, and Leppert M. A novel potassium channel gene, KCNQ2, is mutated in an inherited epilepsy of newborns. *Nat Genet* 18: 25-29, 1998.

Suh BC and Hille B. Recovery from muscarinic modulation of M current channels requires phosphatidylinositol 4,5-bisphosphate synthesis. *Neuron* 35: 507-520, 2002.

Suh BC, Horowitz LF, Hirdes W, Mackie K, and Hille B. Regulation of KCNQ2/KCNQ3 current by G protein cycling: the kinetics of receptor-mediated signaling by Gq. *J Gen Physiol* 123: 663-683, 2004.

Thompson SH. Cyclic GMP-gated channels in a sympathetic neuron cell line. *Journal of General Physiology* 110: 155-164, 1997.

Thorne R and Horn JP. Role of ganglionic cotransmission in sympathetic control of the isolated bullfrog aorta. *J Physiol* 498: 201-214, 1997.

Tokimasa T, Simmons MA, Schneider CR, and Akasu T. Hyperpolarizing shift of the M-current activation curve after washout of muscarine in bullfrog sympathetic neurons. *Neurosci Lett* 207: 97-100, 1996.

Tosaka T, Chichibu S, and Libet B. Intracellular analysis of slow inhibitors and excitatory postsynaptic potentials in sympathetic ganglia of the frog. *J Neurophysiol* 31: 396-409, 1968.

Tsuji S and Kuba K. Muscarinic regulation of two ionic currents in the bullfrog sympathetic neurone. *Pflugers Arch* 411: 361-370, 1988.

Wang HS, Pan Z, Shi W, Brown BS, Wymore RS, Cohen IS, Dixon JE, and McKinnon D. KCNQ2 and KCNQ3 potassium channel subunits: molecular correlates of the M-channel. *Science* 282: 1890-1893, 1998.

Weight FF and Votava J. Slow synaptic excitation in sympathetic ganglion cells: evidence for synaptic inactivation of potassium conductance. *Science* 170: 755-758, 1970.

Wheeler DW, Kullmann PH, and Horn JP. Estimating use-dependent synaptic gain in autonomic ganglia by computational simulation and dynamic-clamp analysis. *J Neurophysiol* 92: 2659-2671, 2004.

Zhang H, Craciun LC, Mirshahi T, Rohacs T, Lopes CM, Jin T, and Logothetis DE. PIP(2) activates KCNQ channels, and its hydrolysis underlies receptor-mediated inhibition of M currents. *Neuron* 37: 963-975, 2003.

Figure legends

Figure 1. Muscarine enhances the impact of nicotinic EPSPs by reducing threshold-g_{syn}

A Dynamic clamp experiment in which bath application of 1 μM muscarine lowered threshold-g_{syn} by 31%. The lower traces illustrate the synaptic conductance used to drive the dynamic clamp and the upper traces illustrate membrane potential responses that straddle action potential threshold (stippled line), which did not change in the presence of muscarine. Dashed lines indicate 0 mV. **B** Time course of the muscarinic reduction of threshold-g_{syn} of the neuron shown in **A**. Note the transient over-recovery of threshold-g_{syn} after washout of muscarine. **C**, **D** Grouped data from 26 neurons shows that muscarinic reduction of threshold-g_{syn} (**C**) is accompanied by depolarization of V_{rest} (**D**). **E** Scatter plot of the data from individual neurons shows a weak correlation between the muscarinic changes in threshold-g_{syn} and V_{rest}. The straight line is a linear fit to the data points, with the 95% confidence band indicated by dashed lines.

Figure 2. Membrane depolarization does not fully account for the actions of muscarine upon threshold-g_{syn} and fast EPSP waveforms

A Example of a cell where injecting 70 pA of hyperpolarizing current nullified the depolarization produced by muscarine and 330 pA of depolarizing current mimicked the muscarinic depolarization. **B** Grouped data from 7 cells used for the experiment illustrated in panel A. Statistical comparisons were based on ANOVA. **C** Comparison of fast EPSPs produced by a virtual conductance waveform (5 nS peak amplitude). Injected currents were used to nullify the muscarinic depolarization (trace 3) and to mimic it (trace

4). **D** Superimposition of virtual EPSPs at the control resting potential (traces 1 and 3) and the depolarized potential (traces 2 and 4) show that in both cases muscarine had little effect upon peak EPSP amplitude, but prolonged EPSP duration. Note that under control conditions the subthreshold EPSPs in **A** elicit undershoots, which are inhibited by muscarine. This indicates that the EPSPs are not purely passive. In other words, fast EPSPs activate some M-current, which speeds the time course of their decay under control conditions.

Figure 3. Muscarinic excitation arises from I_M and a leak current

A Sympathetic B neurons typically respond to a step depolarizing current (lower trace) by generating a single action potential (upper trace). Bath application of 1 μM muscarine converts the response to one of repetitive firing. Dashed lines indicate 0 mV. In these experiments, two types of steady-state I-V relations were observed (**B**, **C**). Upper graphs illustrate the I-V relations in control Ringer and muscarine. Net muscarinic currents, determined by subtraction, are plotted below. **B** Most cells (92%) responded to muscarine with a non-linear inward current produced by suppression of gK_M at potentials above –70 mV. **C** In three cells muscarine induced two-component responses consisting of an inward linear leak current that decreased as the membrane was depolarized from –120 to –60 mV and the inward M-current response at more depolarized potentials. I-V relations in this figure were constructed from voltage-clamp data using a slow ramp command (9 mV/s) from –30 to –120 mV.

Figure 4. gK_M and g_{leak} interact synergistically to lower threshold-g_{syn}

Panel **A** illustrates the time course of an experiment in which muscarine was used to inhibit gK_M and the dynamic clamp was used to introduce a 0.25 nS virtual g_{leak}. Threshold-g_{syn} was repeatedly measured in the presence (open triangles) and absence (filled diamonds) of the leak. These data show that introducing g_{leak} lowered threshold-g_{syn} and that application of muscarine produced a further decrease in threshold-g_{syn}. Note, however, that the effect of g_{leak} was larger in the presence of muscarine. **B** A similar synergy was observed in 11 experiments where the combination of g_{leak} (0.1 – 1 nS) and muscarine (1 μM) reduced threshold-g_{syn} by about 30% more than expected from the sum of the individual effects. **C** Sorting the data into a group of 11 experiments where synergy >0 was observed and 15 experiments where synergy was absent or slightly negative, revealed that synergy depends on the resting potential. In addition to data from individual experiments, the graph includes the mean ± standard deviation for each group. **D** Injection of constant depolarizing current to shift V_{rest} increased the synergy between g_{leak} and gK_M in 4 of 4 neurons.

Figure 5. Muscarine reproducibly increases synaptic gain

A Time course of synaptic gain (top), threshold-g_{syn} (middle) and V_{rest} (bottom) from a cell that was repeatedly stimulated with a synaptic template incorporating 1 primary and 9 secondary nicotinic synapses, each firing at a mean rate of 5 Hz. During four exposures to muscarine, the strength of the secondary synapses were set to 90% and 50% threshold-g_{syn}. At the end of the experiment the secondary synapses were eliminated by setting their strength to 0. Panel **B** illustrates brief 4 s segments from the synaptic gain measurements denoted **a**-**e** in panel **A**. In each trace, asterisks mark action potentials

elicited by summation of secondary EPSPs and dashed lines indicate 0 mV. By comparing **a** and **b** it can be seen that muscarine increased the number of action potentials driven by secondary synapses - this is the effect that produces the increase of synaptic gain. A similar though smaller effect was observed when the strength of the secondary synapses was reduced from 90% threshold-g_{syn} (**Ba**,**Bb**) to 50% threshold-g_{syn} (**Bc**,**Bd**). Turning off the secondary synapses (**Be**) reduced the gain to slightly below 1. This occurred because some primary EPSPs failed to trigger action potentials due to refractory occlusion between closely timed events. An arrow marks one example of such a failure where two EPSPs were separated by only 3.2 ms.

Figure 6. Muscarine increases synaptic gain over a range of physiologically realistic stimulus parameters

Grouped data from experiments where secondary synaptic strength, the number of secondary synapses (n) and the presynaptic firing rate were systematically varied. In each graph, the number in the black bar (1-5 μM muscarine) denotes the number of cells in the comparison and the gray bar to the left is the paired control. All differences were statistically significant except for that using synapses set to 50% threshold-g_{syn} in panel **C**. See Results for additional details.

Figure 7. Muscarine and g_{leak} interact synergistically to increase synaptic gain

A Ten second segments from longer synaptic gain measurements in a cell that was sequentially tested in control Ringer, after introducing a 0.25 nS virtual g_{leak}, after bath

application of 1 μM muscarine and finally with the combination of added g_{leak} and muscarine. Dashed lines indicate 0 mV and asterisks indicate action potentials triggered by secondary EPSPs. The synaptic template contained 1 primary synapse and 3 secondary synapses scaled to 50% threshold-g_{syn} and firing at mean rates of 0.5 Hz. Comparing the traces reveals that combined stimulation was much more effective than the individual treatments employing the virtual leak and muscarine. **B** The same synergistic enhancement of synaptic gain was seen in pooled data from 5 neurons treated with 1 μM muscarine and 0.25 - 0.5 nS g_{leak}. Synaptic gain measurements were conducted with repeated trials to assure stable conditions during each experiment.

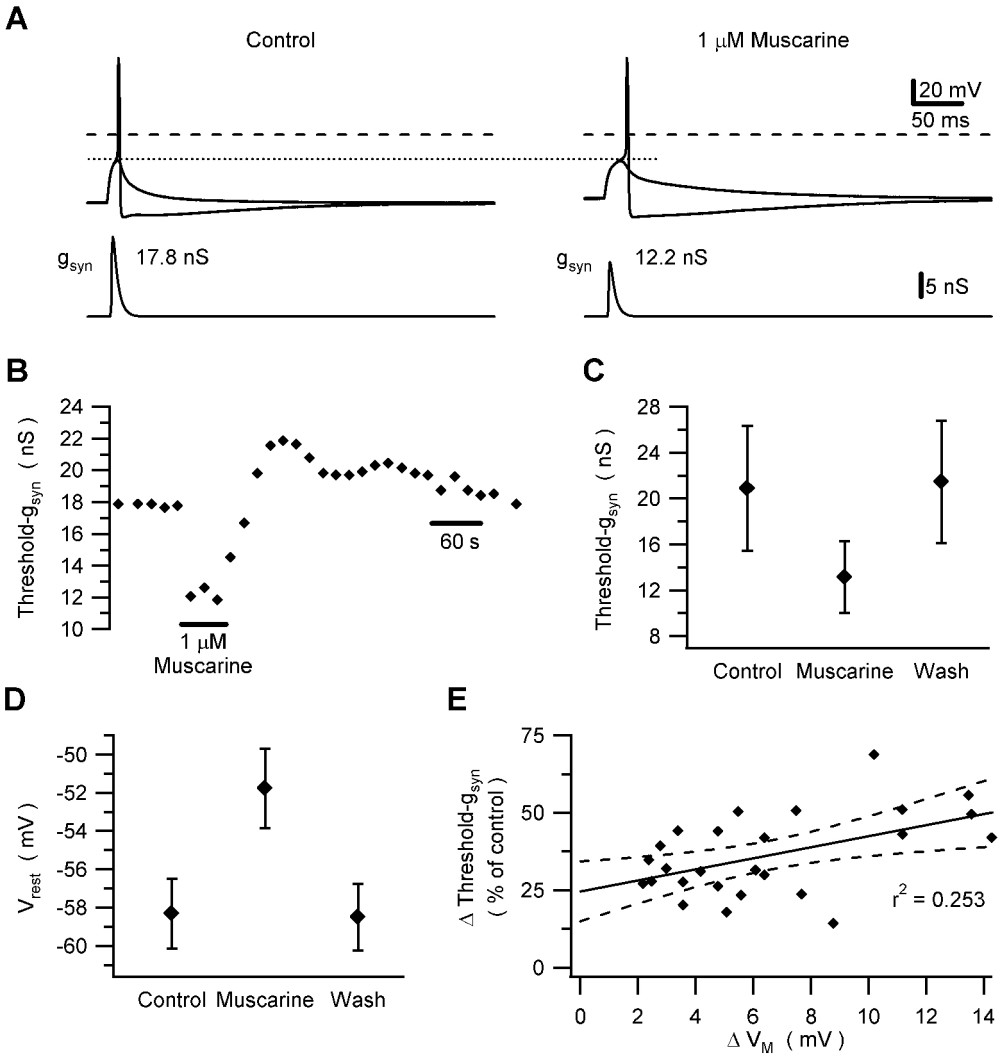
A
Control
1 μM Muscarine
20 mV
50 ms
g_syn
17.8 nS
g_syn
12.2 nS
5 nS
B
Threshold-g_syn (nS)
24
22
20
18
16
14
12
10
60 s
1 μM
Muscarine
C
Threshold-g_syn (nS)
28
24
20
16
12
8
Control
Muscarine
Wash
D
V_rest (mV)
-50
-52
-54
-56
-58
-60
Control
Muscarine
Wash
E
Δ Threshold-g_syn
(% of control)
75
50
25
0
r^2 = 0.253
0
2
4
6
8
10
12
14
Δ V_M (mV)

Figure 1

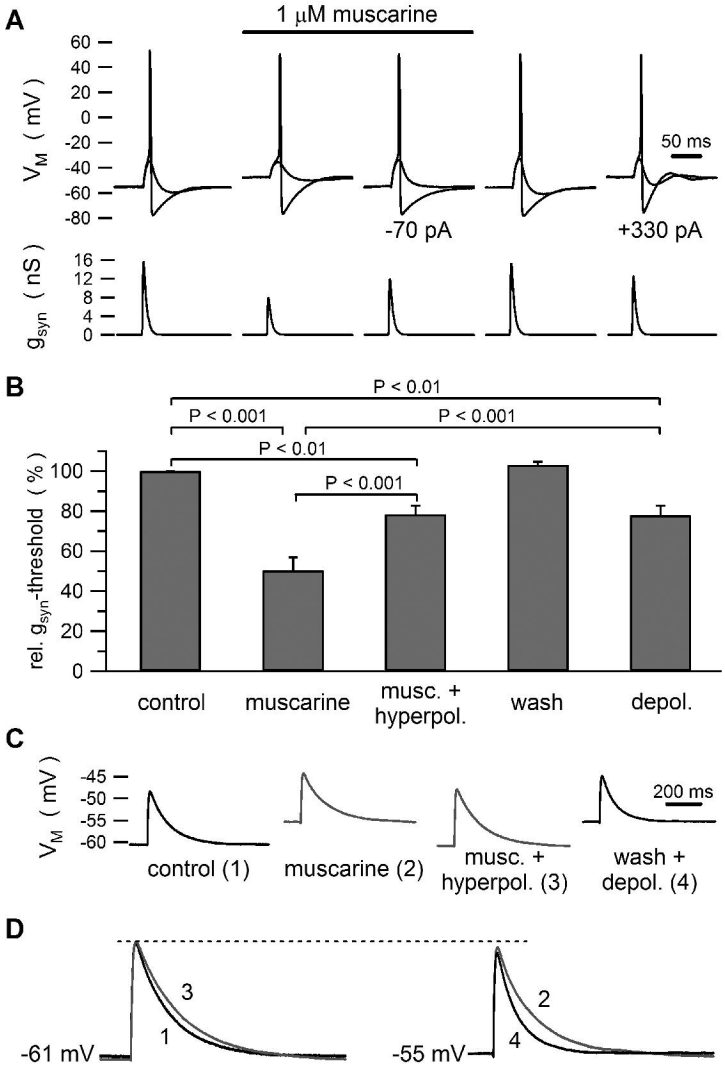
A
1 μM muscarine
60
40
20
0
-20
-40
-60
-80
V_M (mV)
50 ms
-70 pA
+330 pA
16
12
8
4
0
g_{syn} (nS)
B
P < 0.01
P < 0.001
P < 0.001
P < 0.01
P < 0.001
rel. g_{syn}-threshold (%)
100
80
60
40
20
0
control
muscarine
musc. + hyperpol.
wash
depol.
C
-45
-50
-55
-60
V_M (mV)
200 ms
control (1)
muscarine (2)
musc. + hyperpol. (3)
wash + depol. (4)
D
3
1
-61 mV
2
4
-55 mV

Figure 2

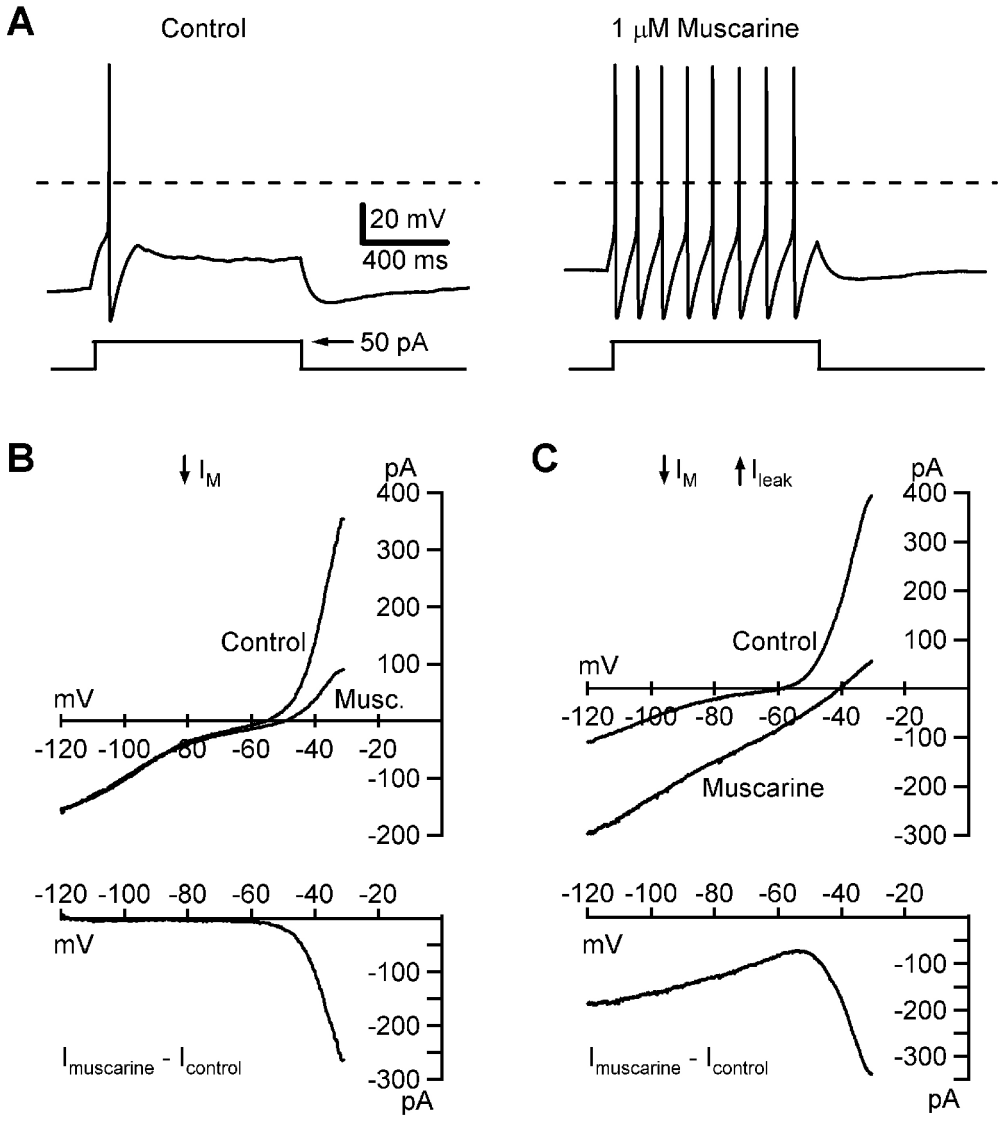
A
Control
1 μM Muscarine
20 mV
400 ms
50 pA
B
↓ I_M
pA
400
300
200
100
Control
mV
Musc.
-120 -100 -80 -60 -40 -20
-100
-200
-120 -100 -80 -60 -40 -20
mV
-100
-200
-300
pA
$I_{muscarine}$ - $I_{control}$
C
↓ I_M
↑ I_{leak}
pA
400
300
200
100
Control
mV
-120 -100 -80 -60 -40 -20
-100
-200
-300
Muscarine
-120 -100 -80 -60 -40 -20
mV
-100
-200
-300
pA
$I_{muscarine}$ - $I_{control}$

Figure 3

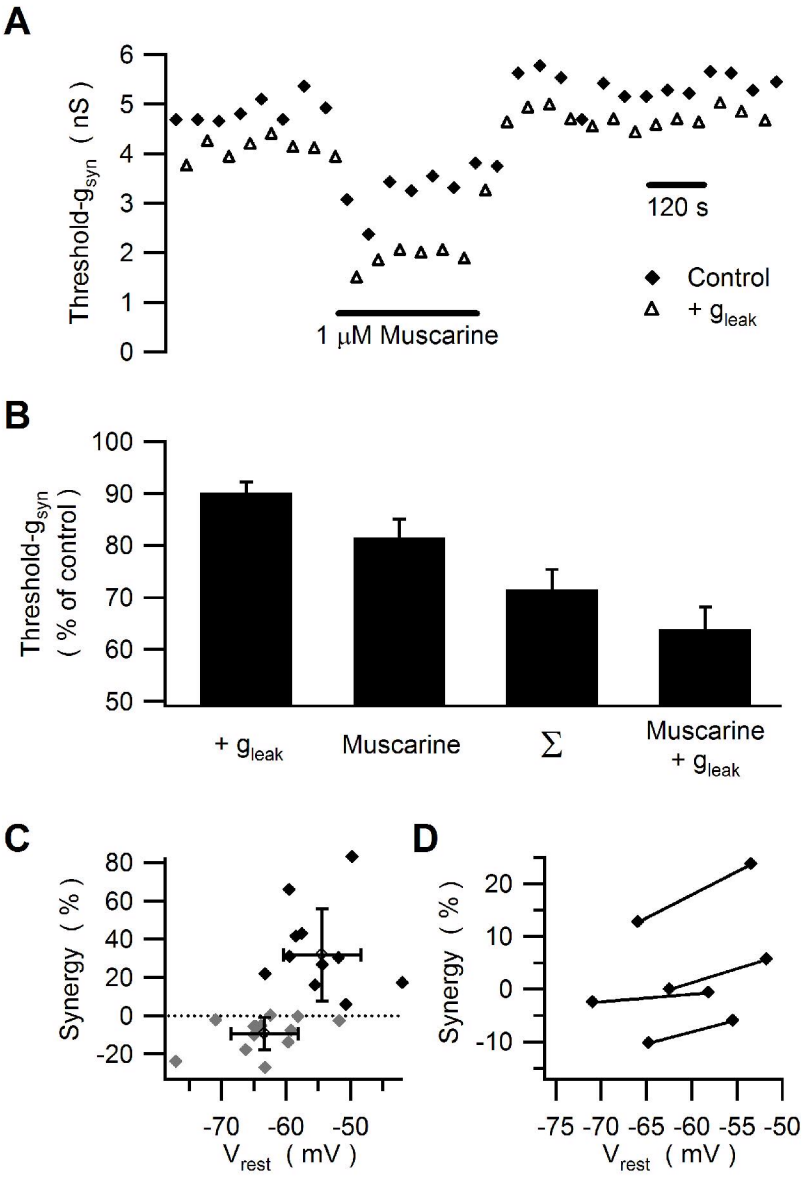
A
Threshold-g_{syn} (nS)
120 s
Control
+ g_{leak}
1 μM Muscarine
B
Threshold-g_{syn}
(% of control)
+ g_{leak}
Muscarine
Σ
Muscarine
+ g_{leak}
C
Synergy (%)
V_{rest} (mV)
D
Synergy (%)
V_{rest} (mV)

Figure 4

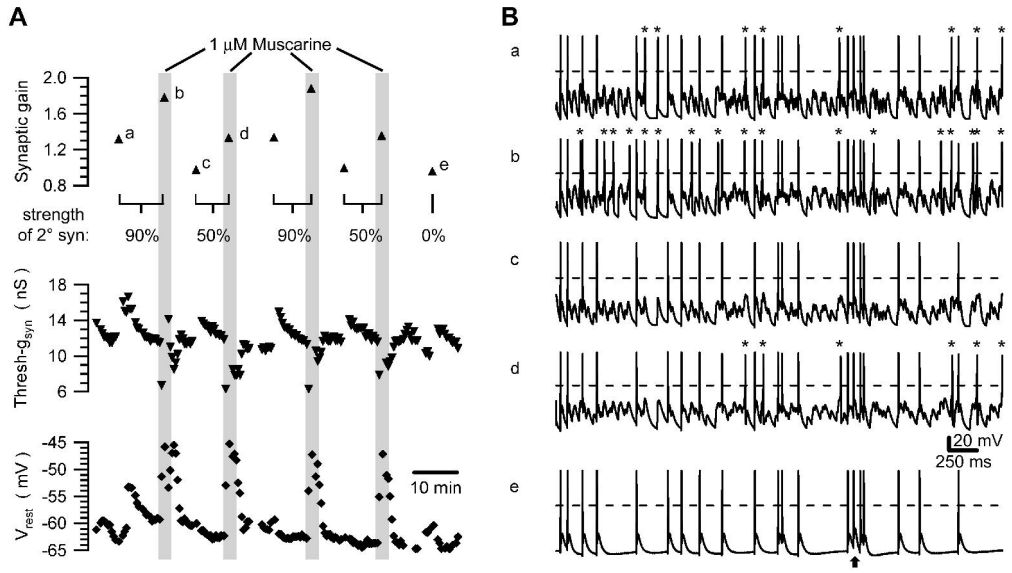
A
1 μM Muscarine
Synaptic gain
2.0
1.6
1.2
0.8
a
b
c
d
e
strength
of 2° syn:
90%
50%
90%
50%
0%
Thresh-g$_{syn}$ (nS)
18
14
10
6
V$_{rest}$ (mV)
-45
-50
-55
-60
-65
10 min
B
a
b
c
d
e
20 mV
250 ms

Figure 5

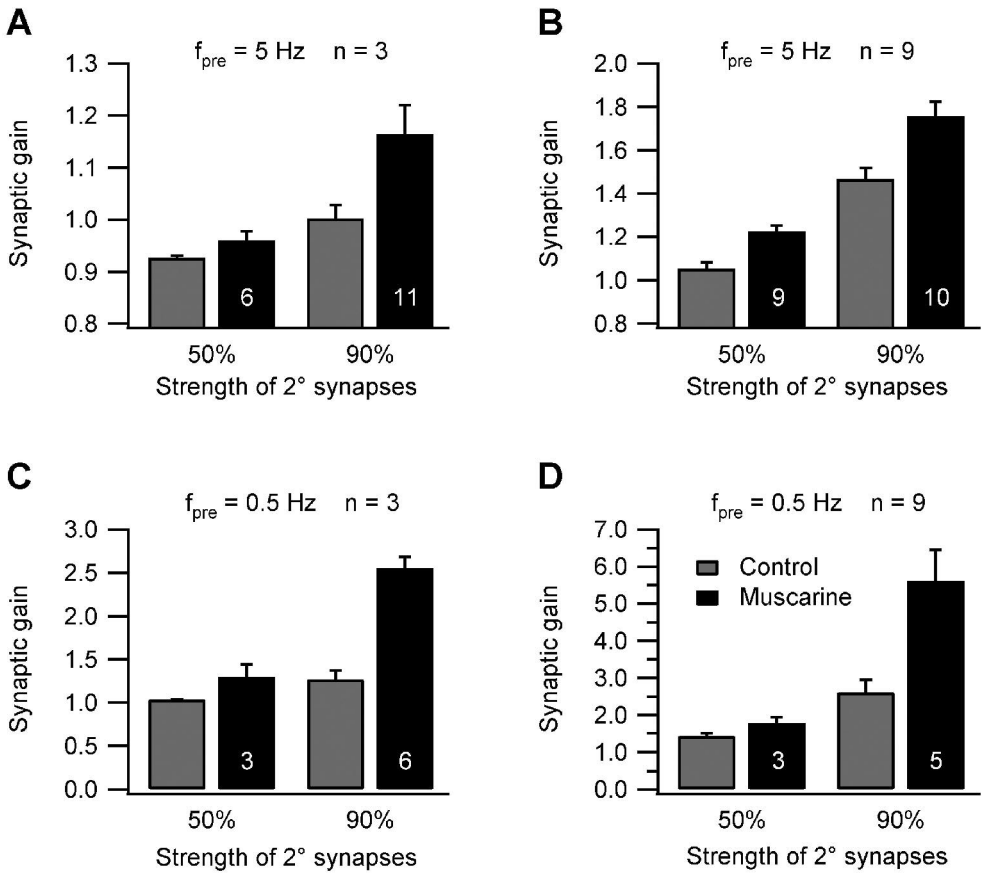
A
f_{pre} = 5 Hz n = 3
Synaptic gain
1.3
1.2
1.1
1.0
0.9
0.8
6
11
50%
90%
Strength of 2° synapses
B
f_{pre} = 5 Hz n = 9
Synaptic gain
2.0
1.8
1.6
1.4
1.2
1.0
0.8
9
10
50%
90%
Strength of 2° synapses
C
f_{pre} = 0.5 Hz n = 3
Synaptic gain
3.0
2.5
2.0
1.5
1.0
0.5
0.0
3
6
50%
90%
Strength of 2° synapses
D
f_{pre} = 0.5 Hz n = 9
Control
Muscarine
Synaptic gain
7.0
6.0
5.0
4.0
3.0
2.0
1.0
0.0
3
5
50%
90%
Strength of 2° synapses

Figure 6

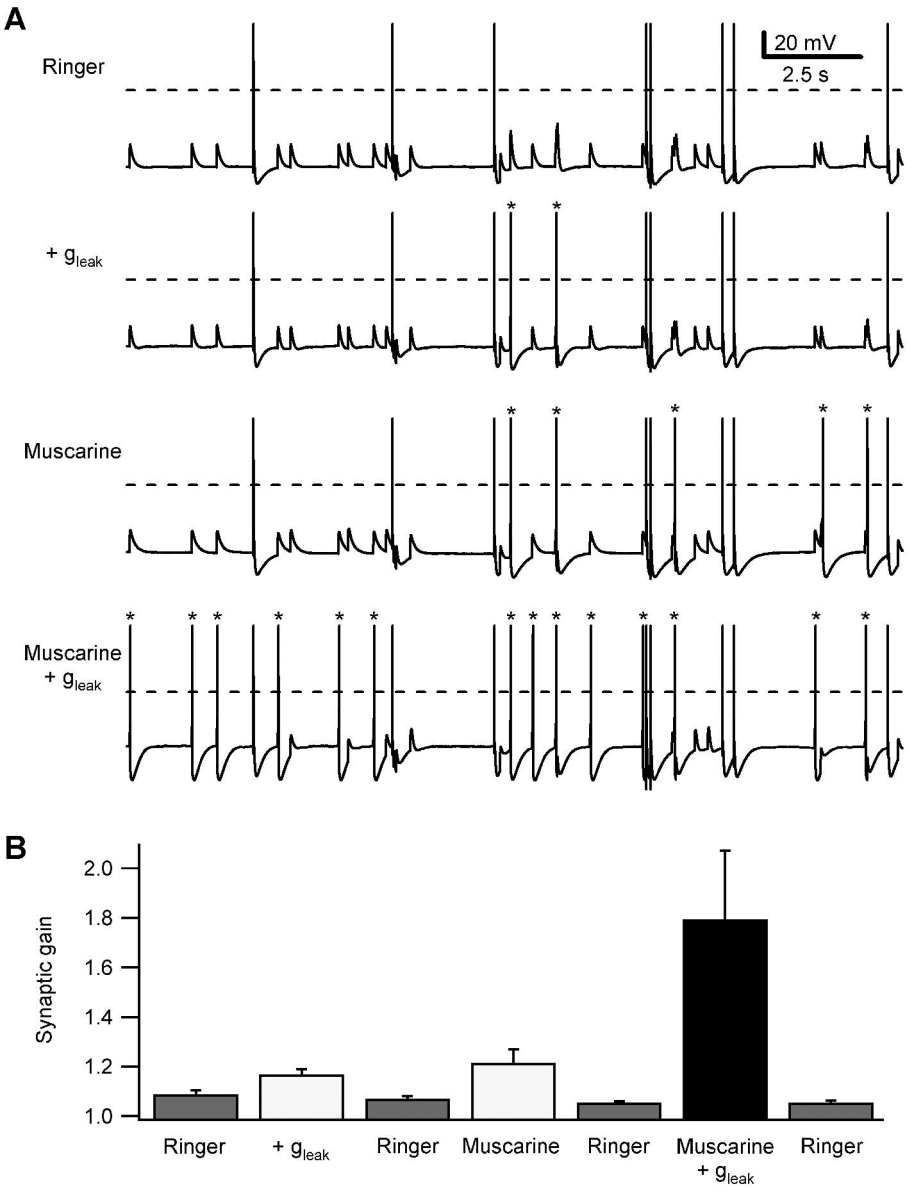
A
Ringer
20 mV
2.5 s
+ g leak
Muscarine
Muscarine
+ g leak
B
Synaptic gain
2.0
1.8
1.6
1.4
1.2
1.0
Ringer
+ g leak
Ringer
Muscarine
Ringer
Muscarine
+ g leak
Ringer

Figure 7